A Physics-Based Compact Model of Stochastic Switching in Spin-Transfer Torque Magnetic Memory

Roberto Carboni, *Student Member, IEEE*, Elena Vernocchi, *Student Member, IEEE*, Manzar Siddik, Jon Harms, Andy Lyle, Gurtej Sandhu, and Daniele Ielmini, *Fellow, IEEE*

***Abstract*— Spin-transfer torque random-access memory (STT-RAM) is gaining momentum as a promising technology for high-density and embedded nonvolatile memory. Owing to random thermal fluctuations, switching transitions generally display statistical variations from cycle to cycle. Stochastic variations are critical to the hindering of memory and computing applications of STT-RAM. To enable the design of STT-RAM circuits for memory and computing, there is a need for accurate compact models capable of predicting the stochastic behavior. Here, we present a detailed model accounting for the anomalous thermal regime of switching deviating from the Néel–Brown thermal model below 200 ns. Anomalous switching is explained by the nonlinear lowering of the energy barrier associated with the perpendicular magnetic anisotropy (PMA). The model is extensively verified against the write-error-rate (WER) data as a function of applied voltage and pulsewidth and experimental switching time-delay distributions.**

***Index Terms*— Magnetic tunnel junction (MTJ), spin-transfer torque magnetoresistive RAM (STT-MRAM), stochastic switching, switching variability modeling.**

I. Introduction

SPIN-TRANSFER TORQUE random-access memory (STT-RAM) is attracting a strong interest because of the storage-class memory (SCM) [1]–[5], dynamic RAM (DRAM) replacement [6], and embedded nonvolatile memory [6]–[8] due to its fast switching [9], nonvolatile states, high endurance [10], CMOS compatibility, and low-current operation [11].

STT-RAM and spintronic devices in general find application also in novel non-von Neumann concepts of computing, e.g., as an electronic synapse in neural networks [12], a nonvolatile logic [13], [14], and a random number generator (RNG) [15]. This boost of applicative interest in STT memory is due to the electronic switching that is crucial to enable high speed, negligible resistance variation, and high endurance [16].

STT magnetic memory is based on the magnetic tunnel junction (MTJ), which consists of a metal–insulator–metal structure comprising a thin MgO tunnel barrier ($t_{MgO} \approx 1$ nm) separating two CoFeB ferromagnetic electrodes (FMs). Having a fixed magnetic polarization, one of these two electrodes is called pinned layer (PL), whereas the free layer (FL) can change its polarization between parallel (P) and antiparallel (AP) with respect to the PL. The MTJ resistance can assume two values depending on the relative orientation of the magnetic polarization of the FL and PL as a result of the tunnel magnetoresistance effect (TMR) [17]. In particular, the P state has a relatively low resistance R_P, while the AP state has a relatively high resistance R_{AP}. Electronic switching between the two states takes place by spin-transfer torque (STT), where the spin-polarized electrons flowing across the MTJ induce a change in the FL magnetic polarization by angular momentum conservation [18], [19]. In particular, perpendicular spin-transfer torque (p-STT), where the polarization of the two FMs is perpendicular to the MTJ plane, shows reduced switching current for the same retention time, thus enabling the low-power operation and improved scalability [20], [21].

In the thermal regime, STT switching takes place by random thermal fluctuations, thus featuring an intrinsically stochastic behavior. While the stochastic switching delay is harmful to the STT memory operation due to random switching variations, it is considered beneficial to true-RNG (TRNG) [15], stochastic computing [22], [23], and brain-inspired computing [24], [25].

Both memory and computing applications require accurate compact models for physics-based simulation of STT-RAM circuits. Previous STT switching models rely on the Landau–Lifshitz–Gilbert (LLG) equation [26], [27], but such numerical approaches are computing-intensive, which makes them unsuitable for electronic circuit simulators. Thus, simple analytical compact models are the ideal candidates for such tasks [28]. However, most analytical switching

Manuscript received May 12, 2019; revised June 27, 2019 and July 29, 2019; accepted August 1, 2019. This work was supported by the European Research Council under Grant ERC-2014-CoG-648635-RESCUE. The review of this article was arranged by Editor J. Kang. *(Corresponding author: Daniele Ielmini.)*

R. Carboni, E. Vernocchi, and D. Ielmini are with the Dipartimento di Elettronica, Informazione e Bioingegneria and Italian Universities Nanoelectronics Team, Politecnico di Milano, 20133 Milan, Italy (e-mail: roberto.carboni@polimi.it; elena.vernocchi@mail.polimi.it; daniele.ielmini@polimi.it).

M. Siddik, J. Harms, A. Lyle, and G. Sandhu are with Micron Technology, Inc., Boise, ID 83707 USA.

Color versions of one or more of the figures in this article are available online at http://ieeexplore.ieee.org.

Digital Object Identifier 10.1109/TED.2019.2933315

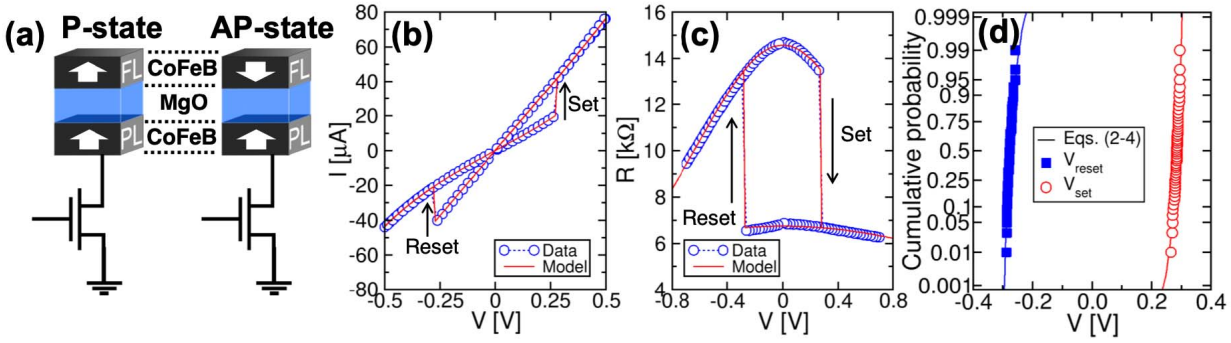

Fig. 1. (a) Perpendicular STT memory device: P state and AP state. (b) Measured *I–V* curve in dc conditions and (c) corresponding *R–V* characteristics evidencing set (AP→P) and reset (P→AP) transitions. (d) Distributions of stochastic switching voltages V_{set} and V_{reset} for 50 dc cycles.

models of STT-RAM are limited to the thermal regime (>200 ns) [29] and the precession regime (<1 ns) [30], while the intermediate regime is only introduced as a mathematical transition [31]–[33]. As a result, the physics involved in the switching behavior for the intermediate regime has not been conclusively addressed [34]–[37]. On the other hand, practical STT-RAM applications mostly work in the intermediate regime [38] due to the relatively large critical current and to prevent time-dependent dielectric breakdown [16].

While the physics of stochastic switching can be described by micromagnetic simulations [37], [39], most analytical approaches consist of empirical functional form fitting that can hardly provide a physical understanding [40], [41]. Moreover, statistical switching models are generally limited to few percentage [32], which is insufficient to predict the memory write error rate (WER) and the operation of stochastic computing primitives.

In this article, we present a physics-based stochastic model of STT memory. The compact model is capable of computing switching probability with 10^{-4} accuracy in the thermal regime (>200 ns) and the intermediate regime (<200 ns). The anomalous thermal regime of switching, deviating from the Néel–Brown thermal model, is attributed to nonlinear lowering of the energy barrier associated with the perpendicular magnetic anisotropy (PMA). The model accounts for WER data of 70 nm STT-RAM as a function of applied voltage for various pulsewidths, accurately reproducing switching-delay distributions.

II. p-STT Sample Characteristics

Fig. 1(a) shows the structure of STT magnetic memory devices used in this study, consisting of a CoFeB PL (bottom electrode, BE) and FL (top electrode, TE) with a crystalline MgO dielectric layer. The device is a p-STT-RAM with an out-of-plane magnetization easy axis with two stable states, namely, a P-state with low resistance and an AP-state with high resistance. The device cross-sectional area is 70 nm × 70 nm. Fig. 1(b) shows the measured current–voltage (*I–V*) characteristics under quasi-static ramped voltage (dc) conditions, where the set event, i.e., AP→P transition, occurred at a positive voltage $V_{set} = 0.27$ V. The reset event, i.e., P→AP transition, occurred at a negative voltage $|V_{reset}| = 0.27$ V,

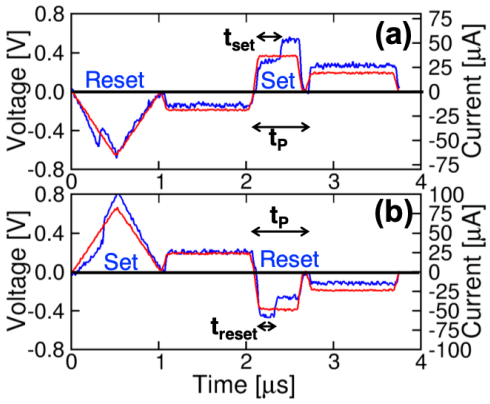

Fig. 2. Applied voltage waveform and corresponding read current traces during a WER experiment for (a) set and (b) reset transitions.

underlining the symmetric switching behavior of our samples. Fig. 1(c) shows the resistance–voltage (*R–V*) curve, where *R* was obtained from Fig. 1(b) as $R = V/I$. The figures also show the calculated conduction characteristics by an analytical model [16]. Cycle-to-cycle repetition of the switching characteristics shows statistical variation of V_{set} and V_{reset}. Fig. 1(d) shows the distributions of stochastic switching voltages V_{set} and V_{reset} for 50 dc cycles.

III. WER Study

To better address the cycle-to-cycle statistical variation of STT switching, we measured the WER (i.e., the failure rate of the switching transition) according to the technique in Fig. 2. For instance, Fig. 2(a) shows the voltage waveform applied to assess the WER of set transition, consisting of: 1) a negative-voltage triangular pulse at $V_{-} = -0.7$ V to deterministically initialize the cell in the AP state; 2) a negative-voltage square pulse for reading the cell state; 3) a positive-voltage square pulse, with amplitude V_A and duration t_P, to induce the stochastic set transition (AP→P); and 4) a positive-voltage square pulse for a final reading to verify the cell state. Both read pulses have an amplitude $|V_{read}| = 0.15$ V, with the same polarity as the previous programming pulse to prevent read disturbs [42]. Pulses (1), (2), and (4) have the same pulsewidth of 1 μs,

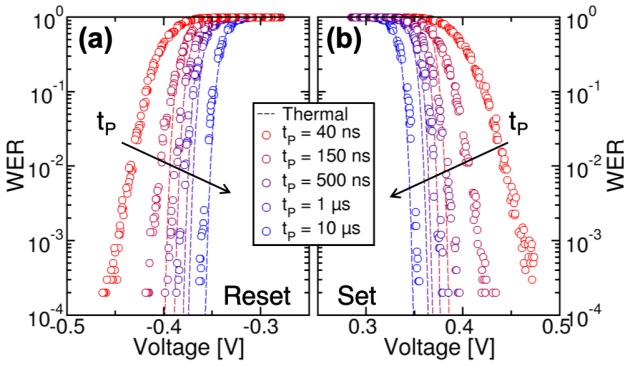

Fig. 3. Measured and calculated WER as a function of the applied voltage for different pulsewidths t_P for (a) reset and (b) set transitions. Data show a slope reduction for shorter t_P, not predicted by the thermal model described by (1) and (2).

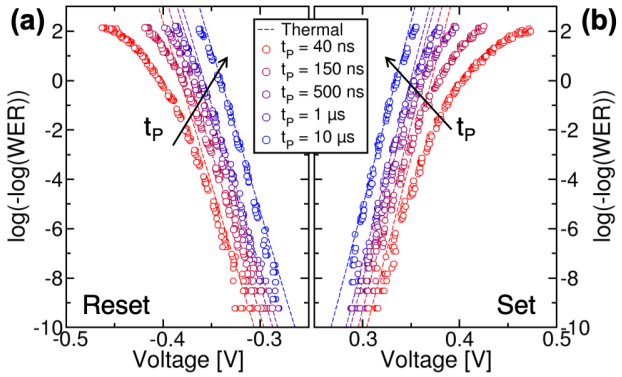

Fig. 4. Voltage distributions in a Weibull plot, i.e., log(−log(WER)), for (a) reset and (b) set transitions. Data show a marked deviation from the expected linear behavior in the thermal regime to an anomalous nonlinear shape for $t_P < 200$ ns.

while the set pulse has a variable pulsewidth t_P ranging from 40 ns to 10 μs. The final state of the cell indicates the success or failure of the transition to P state. The WER can thus be defined as the ratio between the number of failures and the total number of cycles. Note that the current measured with a digital oscilloscope, also shown in Fig. 2(a), allows to assess the set time t_{set} in correspondence with the current rise during the set pulse.

Fig. 2(b) shows a similar waveform for the evaluation of reset WER, consisting of: 1) a positive-voltage triangular pulse of amplitude $V_+ = 0.7$ V to initialize the cell in P state; 2) a positive-voltage square pulse for reading the cell state; and 3) a negative-voltage square pulse with amplitude V_A and duration t_P to induce the stochastic reset transition (P→AP); and (4) a negative-voltage square pulse for the final reading to assess the cell state. The final reading evidences the success or failure of the P→AP transition, thus allowing to evaluate the WER as the ratio of failure events to the total cycles. The reset time t_{reset} can be estimated by the current trace in the figure. To characterize the WER, we repeated the waveforms of Fig. 2 10^4 times for each value of t_P, except for $t_P = 10$ μs, where only 7000 cycles were applied. All measurements were carried out at room temperature.

Fig. 3 shows the measured WER as a function of the voltage V applied during the stochastic square pulse for (a) reset transition and (b) set transition at increasing pulsewidth t_P. The WER drops almost exponentially at increasing voltage. As t_P decreases, the transition to low WER occurs at the increasing voltage and with decreasing slope. The same data of Fig. 3 are reported in Fig. 4 in a Weibull scale, namely, log(−log(WER)), for (a) reset transition and (b) set transition at increasing t_P. These results indicate that the set/reset voltages obey a Weibull distribution, at least in the thermal regime ($t_P > 200$ ns) where data appear as a straight line in the Weibull plot. As t_P decreases, the distributions indicate a marked deviation from the Weibull distribution [43]. Such deviation with respect to the thermal regime is consistent with the observation in [35] and [43] for $t_P < 600$ ns. A t_P-dependent WER slope, similar to our data in Fig. 3, was also reported in previous WER studies [44], [45], although no detailed physical explanation or modeling were given. A similar behavior, resulting in a larger than predicted WER at short t_P, was evidenced in the presence of back-hopping and low-probability bifurcated switching (LPBS) [46], [47]. However, thanks to our technique providing a real-time monitoring of the device current, we can rule out any possible back-hopping or LPBS in our measurements.

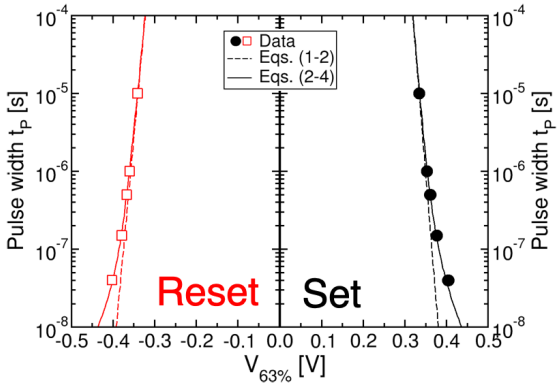

Fig. 5. Measured and calculated Weibull scale parameter $V_{63\%}$ for set and reset at different pulsewidths t_P.

IV. Modeling of Stochastic Switching

Data in Fig. 4 are summarized in Fig. 5, showing the Weibull scale parameter $V_{63\%}$, defined as the voltage for WER = 63%, corresponding to log(−log(WER)) = 0, as a function of t_P. The behavior of the transition voltage $V_{63\%}$ in Fig. 5 is usually explained by the thermal model in Fig. 6 describing the potential energy profile for the transition between P and AP states. The potential energy profile features two wells, corresponding to P and AP states, separated by an energy barrier E_A originating from the PMA in the MTJ. Referring to the AP→P transition, the FL magnetic polarization experiences thermal fluctuations within the AP well, eventually inducing the transition across the energy barrier E_A, as shown in Fig. 6(a). By applying a voltage across the device, the spin-polarized current induces a spin-transfer torque on the FL causing an energy unbalance between the AP and P states, as shown Fig. 6(b) [48], [49]. Thus, the current-driven spin

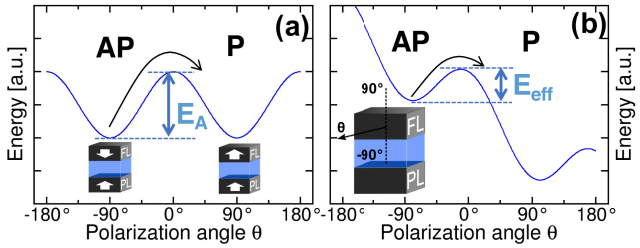

Fig. 6. Illustration of the PMA energy profile as a function of the FL magnetic polarization angle θ. Thermal fluctuations induce AP→P transition across the energy barrier (a) with no applied voltage or (b) with positive applied voltage. The energy unbalance between AP and P states originates from the current-induced STT [48], [49].

TABLE I
SUMMARY OF SWITCHING MODEL PARAMETERS IN (1)–(4)

Parameter	Set	Reset
τ_0 [ns]	1	1
Δ	59.3	54
Δ'	84	84
V_{c0} [mV]	395	410
V_{c0}' [mV]	280	280

torque causes the lowering of the PMA barrier E_A, which accelerates the transition to the P-state [43]. Assuming a linear voltage-induced barrier lowering [43], [50], the characteristic switching time is given by

$$\tau_{th} = \tau_0 e^{\Delta\left(1-\frac{V}{V_{c0}}\right)} \quad (1)$$

where $\Delta = E_A/kT$, while τ_0 and V_{c0} are constant [43]. The WER can thus be obtained by a Poissonian switching probability P given by

$$\frac{dP}{dt} = \frac{(1-P)}{\tau} \quad (2)$$

where τ is the characteristic switching time equal to τ_{th}.

Equations (1) and (2) describe the thermally activated magnetization reversal of a single magnetic domain in the presence of spin-transfer torques. Here, the STT effect is included in the classical Néel–Brown formula [51] by introducing an effective activation energy $E_{eff} = E_A * (1 - V/V_{c0})$ to replace the true energy barrier E_A [29], [52]. Note that the same effect can be described by introducing an effective temperature $T_{eff} = T * (1 - V/V_{c0})^{-1}$ to replace the true lattice temperature [29], [52].

The calculations by (1) and (2) are reported in Figs. 3–5 using parameters from Table I. The calculation results indicate that the thermal model can account for the linear decrease of WER in the Weibull plot of Fig. 4 and the logarithmic decrease of $V_{63\%}$ in Fig. 5, both with slope Δ/V_{c0}, which controls the voltage-induced barrier lowering. However, the thermal model cannot explain the deviation from the linear behavior at $t_P < 200$ ns. To better understand the origin of the nonthermal behavior, we analyzed in Fig. 7 the Weibull shape factor, namely, the derivative of the Weibull distribution in Fig. 4 given by dlog(−log(WER))/dV. The Weibull shape factor, which can be taken as a measure of the barrier lowering coefficient, is plotted as a function of V, and compared with the ideal value Δ/V_{c0} from (1) and (2). Fig. 7 shows that the Weibull shape factor has a t_P-independent universal behavior, being close to Δ/V_{c0} at low V, then sharply decreasing above a critical voltage $V^* \sim 0.33$ V, which suggests a voltage-dependent barrier lowering coefficient. This is in stark contrast with respect to the thermal model predicting a V-independent barrier lowering coefficient Δ/V_{c0}.

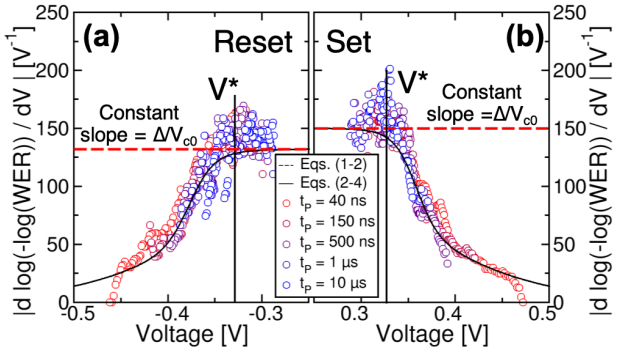

Fig. 7. Experimental and calculated Weibull shape factor dlog(−log(WER))/dV as a function of voltage, for both (a) reset and (b) set transitions, showing a drop in the barrier-lowering coefficient after a critical V^*, with respect to the thermal model value Δ/V_{c0}.

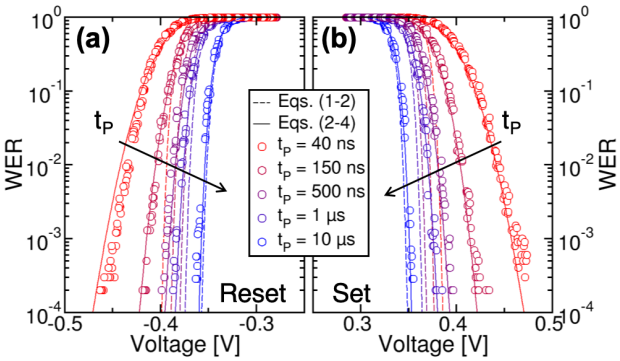

Fig. 8. Measured and calculated WER as a function of the applied voltage for different pulsewidths t_P for (a) reset and (b) set transitions. Calculations in (2)–(4) correctly account for the anomalous WER.

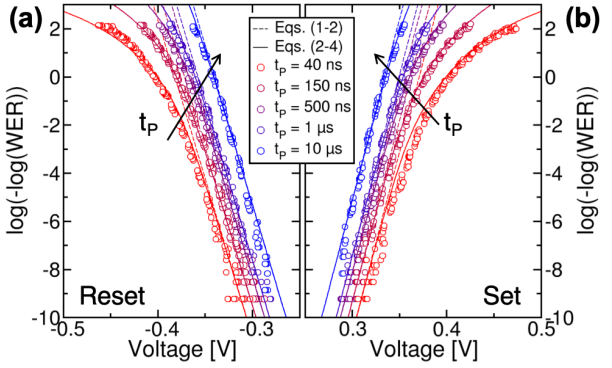

Fig. 9. Voltage distributions in a Weibull plot, i.e., log(−log(WER)), for (a) reset and (b) set transitions. The anomalous deviation for $t_P < 200$ ns is correctly described by (2)–(4).

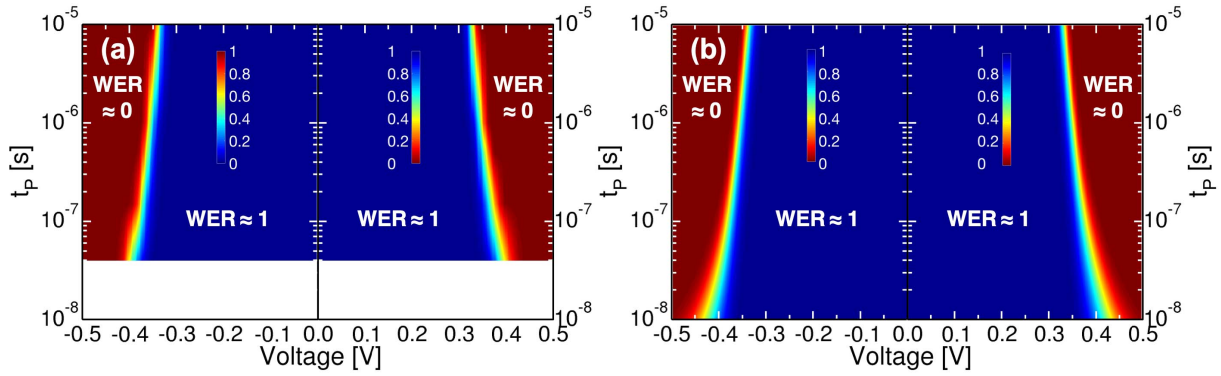

Fig. 10. (a) Experimental and (b) simulated Shmoo diagrams for STT switching. Color plots indicate WER (blue = high WER, red = low WER) for different pairs of applied voltage and pulsewidth.

To account for the anomalous barrier lowering at high voltage, we rewrote the characteristic switching time τ in (2) as

$$\tau = \tau_{\text{th}} + \tau'_{\text{th}} \tag{3}$$

where τ'_{th} is an additional characteristic time given by

$$\tau'_{\text{th}} = \tau_0 e^{\Delta'\left(1-\text{erf}\left(\frac{V}{V'_{c0}}\right)\right)} \tag{4}$$

where parameters Δ' and V'_{c0} are given in Table I, and *erf* is the error function. The error function in (4) allowed to accurately describe the smooth step-like behavior of the Weibull shape factor in Fig. 7, correctly considering its voltage dependence. According to (3) and (4), the energy barrier lowering decreases at high V with respect to the thermal model, thus resulting in the STT transition slowing down compared with the thermal model.

The observed deviation from the thermal regime can thus be viewed as a nonlinear V-induced barrier lowering, similar to a reduced spin-transfer torque efficiency at high voltage [53]. Such effect cannot be neglected in order to accurately account for the intermediate regime between the thermal regime and the precession regime.

V. Simulation Results

Simulation results by (2), (3), and (4) show excellent agreement with the experimental $V_{63\%}$ in Fig. 5 and the Weibull shape factor in Fig. 7, thus supporting the accuracy of our model in describing the anomalous deviation from the thermal model below 200 ns. Fig. 8 shows the measured and calculated WER, which is replotted in Fig. 9 in Weibull scale. Calculations by (2), (3), and (4) correctly describe the deviation at high voltage and relatively short t_{P} in the intermediate regime.

Fig. 10(a) and (b) shows the color plot of the measured WER and calculations by (2), (3), (4), respectively, as a function of V and t_{P}. Calculations well account for the nonlinear transition region between WER = 1 and WER = 0, which plays a crucial role in the design and operation of the STT-RAM device. Fig. 11 shows the Weibull distribution of measured and calculated t_{set} and t_{reset} in Fig. 2 for $t_{\text{P}} = 10\ \mu$s and increasing amplitude V. The transition times were

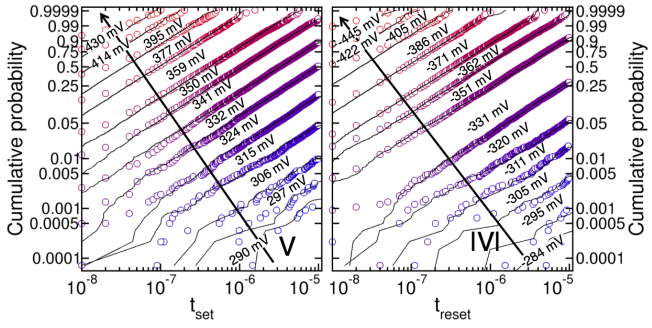

Fig. 11. Measured and calculated t_{set} and t_{reset} Weibull distributions for various values of applied amplitude V.

calculated by a Monte Carlo model of (2). The Monte Carlo simulations well account for both the slope and the voltage dependence of the distributions.

Combining the switching model with an analytical conduction model [16], quasi-static I–V and R–V curves can be simulated with their corresponding distributions of V_{set} and V_{reset}, as shown by calculations in Fig. 1.

VI. Conclusion

This article presents a new physics-based compact model for stochastic switching in STT-RAM. The model combines simplicity (three equations and five free parameters) and accuracy in computing WER, switching voltages, and switching times for both the thermal regime (>200 ns) and the intermediate regime (<200 ns) where deviation from the classical thermal-activated switching regime is observed. Thanks to its simple structure, the model features straightforward portability to other MTJ technologies and easy integration in commercial circuital simulators. The model can support the design of embedded STT memory and novel hardware-primitives for TRNG and stochastic computing.

Acknowledgment

The authors would like to thank W. Kula and W. Chen for discussions.

REFERENCES

[1] S.-W. Chung *et al.*, "4Gbit density STT-MRAM using perpendicular MTJ realized with compact cell structure," in *IEDM Tech. Dig.*, Dec. 2016, pp. 27.1.1–27.1.4. doi: 10.1109/IEDM.2016.7838490.

[2] R. F. Freitas and W. W. Wilcke, "Storage-class memory: The next storage system technology," *IBM J. Res. Develop.*, vol. 52, nos. 4–5, pp. 439–447, 2008. doi: 10.1147/rd.524.0439.

[3] M. Natsui *et al.*, "Nonvolatile logic-in-memory array processor in 90 nm MTJ/MOS achieving 75% leakage reduction using cycle-based power gating," in *IEEE Int. Solid-State Circuits Conf. (ISSCC) Dig. Tech. Papers*, Feb. 2013, pp. 194–195. doi: 10.1109/ISSCC.2013.6487696.

[4] H.-S. P. Wong and S. Salahuddin, "Memory leads the way to better computing," *Nature Nanotechnol.*, vol. 10, no. 3, pp. 191–194, 2015. doi: 10.1038/nnano.2015.29.

[5] T. Endoh, H. Koike, S. Ikeda, T. Hanyu, and H. Ohno, "An overview of nonvolatile emerging memories—Spintronics for working memories," *IEEE J. Emerg. Sel. Topics Circuits Syst.*, vol. 6, no. 2, pp. 109–119, Jun. 2016. doi: 10.1109/JETCAS.2016.2547704.

[6] K. Ikegami *et al.*, "Low power and high density STT-MRAM for embedded cache memory using advanced perpendicular MTJ integrations and asymmetric compensation techniques," in *IEDM Tech. Dig.*, Dec. 2014, pp. 28.1.1–28.1.4. doi: 10.1109/IEDM.2014.7047123.

[7] D. Shum *et al.*, "CMOS-embedded STT-MRAM arrays in 2× nm nodes for GP-MCU applications," in *Proc. Symp. VLSI Technol.*, Jun. 2017, pp. T208–T209. doi: 10.23919/VLSIT.2017.7998174.

[8] S. Ghosh *et al.*, "Overview of circuits, systems, and applications of spintronics," *IEEE J. Emerg. Sel. Topics Circuits Syst.*, vol. 6, no. 3, pp. 265–278, Sep. 2016. doi: 10.1109/JETCAS.2016.2601310.

[9] J. J. Nowak *et al.*, "Dependence of voltage and size on write error rates in spin-transfer torque magnetic random-access memory," *IEEE Magn. Lett.*, vol. 7, 2016, Art. no. 3102604. doi: 10.1109/LMAG.2016.2539256.

[10] R. Carboni *et al.*, "Modeling of breakdown-limited endurance in spin-transfer torque magnetic memory under pulsed cycling regime," *IEEE Trans. Electron Devices*, vol. 65, no. 6, pp. 2470–2478, Jun. 2018. doi: 10.1109/TED.2018.2822343.

[11] D. Apalkov, B. Dieny, and J. M. Slaughter, "Magnetoresistive random access memory," *Proc. IEEE*, vol. 104, no. 10, pp. 1796–1830, Oct. 2016. doi: 10.1109/JPROC.2016.2590142.

[12] S. Lequeux *et al.*, "A magnetic synapse: Multilevel spin-torque memristor with perpendicular anisotropy," *Sci. Rep.*, vol. 6, p. 31510, Aug. 2016. doi: 10.1038/srep31510.

[13] H. Mahmoudi, T. Windbacher, V. Sverdlov, and S. Selberherr, "Implication logic gates using spin-transfer-torque-operated magnetic tunnel junctions for intrinsic logic-in-memory," *Solid-State Electron.*, vol. 84, pp. 191–197, Jun. 2013. doi: 10.1016/j.sse.2013.02.017.

[14] E. Deng, Y. Zhang, J.-O. Klein, D. Ravelsona, C. Chappert, and W. Zhao, "Low power magnetic full-adder based on spin transfer torque MRAM," *IEEE Trans. Magn.*, vol. 49, no. 9, pp. 4982–4987, Sep. 2013. doi: 10.1109/TMAG.2013.2245911.

[15] R. Carboni *et al.*, "Random number generation by differential read of stochastic switching in spin-transfer torque memory," *IEEE Electron Device Lett.*, vol. 39, no. 7, pp. 951–954, Jul. 2018. doi: 10.1109/LED.2018.2833543.

[16] R. Carboni *et al.*, "Understanding cycling endurance in perpendicular spin-transfer torque (p-STT) magnetic memory," in *IEDM Tech. Dig.*, Dec. 2016, pp. 21.6.1–21.6.4. doi: 10.1109/IEDM.2016.7838468.

[17] C. Chappert, A. Fert, and F. N. van Dau, "The emergence of spin electronics in data storage," in *Nanoscience and Technology: A Collection of Reviews From Nature Journals*. Singapore: World Scientific, 2010, pp. 147–157. doi: 10.1038/nmat2024.

[18] J. C. Slonczewski, "Current-driven excitation of magnetic multilayers," *J. Magn. Magn. Mater.*, vol. 159, nos. 1–2, pp. L1–L7, 1996. doi: 10.1016/0304-8853(96)00062-5.

[19] L. Berger, "Emission of spin waves by a magnetic multilayer traversed by a current," *Phys. Rev. B, Condens. Matter*, vol. 54, no. 13, p. 9353, 1996. doi: 10.1103/PhysRevB.54.9353.

[20] S. Ikeda *et al.*, "A perpendicular-anisotropy CoFeB–MgO magnetic tunnel junction," *Nature Mater.*, vol. 9, no. 9, pp. 721–724, 2010. doi: 10.1038/nmat2804.

[21] H. Sato, S. Ikeda, and H. Ohno, "Magnetic tunnel junctions with perpendicular easy axis at junction diameter of less than 20 nm," *Jpn. J. Appl. Phys.*, vol. 56, no. 8, 2017, Art. no. 0802A6. doi: 10.7567/JJAP.56.0802A6.

[22] Y. Lv and J.-P. Wang, "A single magnetic-tunnel-junction stochastic computing unit," in *IEDM Tech. Dig.*, Dec. 2017, pp. 36.2.1–36.2.4. doi: 10.1109/IEDM.2017.8268504.

[23] S. Gaba, P. Sheridan, J. Zhou, S. Choi, and W. Lu, "Stochastic memristive devices for computing and neuromorphic applications," *Nanoscale*, vol. 5, no. 13, pp. 5872–5878, 2013. doi: 10.1039/C3NR01176C.

[24] J. Grollier, D. Querlioz, and M. D. Stiles, "Spintronic nanodevices for bioinspired computing," *Proc. IEEE*, vol. 104, no. 10, pp. 2024–2039, Oct. 2016. doi: 10.1109/JPROC.2016.2597152.

[25] G. Pedretti *et al.*, "Stochastic learning in neuromorphic hardware via spike timing dependent plasticity with RRAM synapses," *IEEE J. Emerg. Sel. Topics Circuits Syst.*, vol. 8, no. 1, pp. 77–85, Feb. 2017. doi: 10.1109/JETCAS.2017.2773124.

[26] F. O. Heinz and L. Smith, "Fast simulation of spin transfer torque devices in a general purpose TCAD device simulator," in *Proc. Int. Conf. Simulation Semiconductor Processes Devices (SISPAD)*, Sep. 2013, pp. 127–130. doi: 10.1109/SISPAD.2013.6650591.

[27] N. Xu *et al.*, "Physics-based compact modeling framework for state-of-the-art and emerging STT-MRAM technology," in *IEDM Tech. Dig.*, Dec. 2015, pp. 28.5.1–28.5.4. doi: 10.1109/IEDM.2015.7409789.

[28] D. Ielmini and V. Milo, "Physics-based modeling approaches of resistive switching devices for memory and in-memory computing applications," *J. Comput. Electron.*, vol. 16, no. 4, pp. 1121–1143, 2017. doi: 10.1007/s10825-017-1101-9.

[29] Z. Li and S. Zhang, "Thermally assisted magnetization reversal in the presence of a spin-transfer torque," *Phys. Rev. B, Condens. Matter*, vol. 69, no. 13, 2004, Art. no. 134416. doi: 10.1103/PhysRevB.69.134416.

[30] J. Z. Sun, "Spin-current interaction with a monodomain magnetic body: A model study," *Phys. Rev. B, Condens. Matter*, vol. 62, no. 1, p. 570, 2000. doi: 10.1103/PhysRevB.62.570.

[31] H. Lim, S. Lee, and H. Shin, "Unified analytical model for switching behavior of magnetic tunnel junction," *IEEE Electron Device Lett.*, vol. 35, no. 2, pp. 193–195, Feb. 2014. doi: 10.1109/LED.2013.2293598.

[32] A. F. Vincent, N. Locatelli, J. O. Klein, W. S. Zhao, S. Galdin-Retailleau, and D. Querlioz, "Analytical macrospin modeling of the stochastic switching time of spin-transfer torque devices," *IEEE Trans. Electron Devices*, vol. 62, no. 1, pp. 164–170, Jan. 2015. doi: 10.1109/TED.2014.2372475.

[33] A. Raychowdhury, D. Somasekhar, T. Karnik, and V. De, "Design space and scalability exploration of 1T-1STT MTJ memory arrays in the presence of variability and disturbances," in *IEDM Tech. Dig.*, Dec. 2009, pp. 1–4. doi: 10.1109/IEDM.2009.5424242.

[34] Y. Zhang *et al.*, "Electrical modeling of stochastic spin transfer torque writing in magnetic tunnel junctions for memory and logic applications," *IEEE Trans. Magn.*, vol. 49, no. 7, pp. 4375–4378, Jul. 2013. doi: 10.1109/TMAG.2013.2242257.

[35] Z. Diao *et al.*, "Spin-transfer torque switching in magnetic tunnel junctions and spin-transfer torque random access memory," *J. Phys., Condens. Matter*, vol. 19, no. 16, 2007, Art. no. 165209. doi: 10.1088/0953-8984/19/16/165209.

[36] R. De Rose *et al.*, "A compact model with spin-polarization asymmetry for nanoscaled perpendicular MTJs," *IEEE Trans. Electron Devices*, vol. 64, no. 10, pp. 4346–4353, Oct. 2017. doi: 10.1109/TED.2017.2734967.

[37] Y. Xie, B. Behin-Aein, and A. W. Ghosh, "Fokker—Planck study of parameter dependence on write error slope in spin-torque switching," *IEEE Trans. Electron Devices*, vol. 64, no. 1, pp. 319–324, Jan. 2017. doi: 10.1109/TED.2016.2632438.

[38] B. Dieny, R. B. Goldfarb, and K.-J. Lee, *Introduction to Magnetic Random-Access Memory*. Hoboken, NJ, USA: Wiley, 2016.

[39] U. Roy, T. Pramanik, L. F. Register, and S. K. Banerjee, "Write error rate of spin-transfer-torque random access memory including micromagnetic effects using rare event enhancement," *IEEE Trans. Magn.*, vol. 52, no. 10, pp. 1–6, Oct. 2016. doi: 10.1109/TMAG.2016.2580532.

[40] G. Siracusano *et al.*, "Description of statistical switching in perpendicular STT-MRAM within an analytical and numerical micromagnetic framework," *IEEE Trans. Magn.*, vol. 54, no. 5, May 2018, Art. no. 1400210. doi: 10.1109/TMAG.2018.2799856.

[41] I.-Y. Im and S.-G. Park, "A read–write circuit for STT-MRAM with stochastic switchings," *IEEE Trans. Magn.*, vol. 54, no. 5, May 2018, Art. no. 3400607. doi: 10.1109/TMAG.2018.2795542.

[42] H. Naeimi, C. Augustine, A. Raychowdhury, S.-L. Lu, and J. Tschanz, "STTRAM scaling and retention failure," *Intel Technol. J.*, vol. 17, no. 1, pp. 54–75, 2013.

[43] R. Heindl, W. H. Rippard, S. E. Russek, M. R. Pufall, and A. B. Kos, "Validity of the thermal activation model for spin-transfer torque switching in magnetic tunnel junctions," *J. Appl. Phys.*, vol. 109, no. 7, 2011, Art. no. 073910. doi: 10.1063/1.3562136.

[44] Z. Wang, Y. Zhou, J. Zhang, and Y. Huai, "Bit error rate investigation of spin-transfer-switched magnetic tunnel junctions," *Appl. Phys. Lett.*, vol. 101, no. 14, 2012, Art. no. 142406. doi: 10.1063/1.4756787.

[45] R. Heindl, W. H. Rippard, S. E. Russek, and A. B. Kos, "Physical limitations to efficient high-speed spin-torque switching in magnetic tunnel junctions," *Phys. Rev. B, Condens. Matter*, vol. 83, no. 5, 2011, Art. no. 054430. doi: 10.1103/PhysRevB.83.054430.

[46] T. Min, J. Z. Sun, R. Beach, D. Tang, and P. Wang, "Back-hopping after spin torque transfer induced magnetization switching in magnetic tunneling junction cells," *J. Appl. Phys.*, vol. 105, no. 7, 2009, Art. no. 07D126. doi: 10.1063/1.3063672.

[47] T. Min *et al.*, "A study of write margin of spin torque transfer magnetic random access memory technology," *IEEE Trans. Magn.*, vol. 46, no. 6, pp. 2322–2327, Jun. 2010. doi: 10.1109/TMAG.2010.2043069.

[48] K. Munira and P. B. Visscher, "Calculation of energy-barrier lowering by incoherent switching in spin-transfer torque magnetoresistive random-access memory," *J. Appl. Phys.*, vol. 117, no. 17, 2015, Art. no. 17B710. doi: 10.1063/1.4908153.

[49] T. Saito, K. Ito, H. Honjo, S. Ikeda, and T. Endoh, "Novel method of evaluating accurate thermal stability for MTJs using thermal disturbance and its demonstration for single-/double-interface p-MTJ," *IEEE Trans. Magn.*, vol. 54, no. 4, Apr. 2018, Art. no. 3400505. doi: 10.1109/TMAG.2017.2688440.

[50] D. C. Ralph, Y.-T. Cui, L. Q. Liu, T. Moriyama, C. Wang, and R. A. Buhrman, "Spin-transfer torque in nanoscale magnetic devices," *Philos. Trans. Roy. Soc. A, Math., Phys. Eng. Sci.*, vol. 369, no. 1951, pp. 3617–3630, 2011. doi: 10.1098/rsta.2011.0169.

[51] W. F. Brown, Jr., "Thermal fluctuations of a single-domain particle," *Phys. Rev.*, vol. 130, p. 1677, Jun. 1963. doi: 10.1103/PhysRev.130.1677.

[52] D. M. Apalkov and P. B. Visscher, "Spin-torque switching: Fokker-Planck rate calculation," *Phys. Rev. B, Condens. Matter*, vol. 72, no. 18, 2005, Art. no. 180405. doi: 10.1103/PhysRevB.72.180405.

[53] H. Liu *et al.*, "Dynamics of spin torque switching in all-perpendicular spin valve nanopillars," *J. Magn. Magn. Mater.*, vols. 358–359, pp. 233–258, May 2014. doi: 10.1016/j.jmmm.2014.01.061.